The JHF-Kamioka neutrino project

Y. Itow[1], T. Kajita[1], K. Kaneyuki[1], M. Shiozawa[1], Y. Totsuka[1],
Y. Hayato[2], T. Ishida[2], T. Ishii[2], T. Kobayashi[2], T. Maruyama[2],
K. Nakamura[2], Y. Obayashi[2], Y. Oyama[2], M. Sakuda[2], M. Yoshida[2],
S. Aoki[3], T. Hara[3], A. Suzuki[3],
A. Ichikawa[4], T. Nakaya[4], K. Nishikawa[4],
T. Hasegawa[5], K. Ishihara[5], A. Suzuki[5],
A. Konaka[6]

[1] Institute for Cosmic Ray Research, University of Tokyo, Kashiwa, Chiba 277-8582, Japan

[2] Inst. of Particle and Nuclear Studies, High Energy Accelerator Research Org. (KEK), Tsukuba, Ibaraki 305-0801, Japan

[3] Department of Physics, Kobe University, Kobe, Hyogo 657-8501, Japan

[4] Department of Physics, Kyoto University, Kyoto 606-8502, Japan

[5] Department of Physics, Tohoku University, Sendai, Miyagi, 980-8578, Japan

[6] TRIUMF, 4004 Wesbrook Mall, Vancouver, British Columbia, Canada, V6T 2A3

Abstract

The JHF-Kamioka neutrino project is a second generation long base line neutrino oscillation experiment that probes physics beyond the Standard Model by high precision measurements of the neutrino masses and mixing. A high intensity narrow band neutrino beam is produced by secondary pions created by a high intensity proton synchrotron at JHF (JAERI). The neutrino energy is tuned to the oscillation maximum at $\sim$1 GeV for a baseline length of 295 km towards the world largest water Čerenkov detector, Super-Kamiokande. Its excellent energy resolution and particle identification enable the reconstruction of the initial neutrino energy, which is compared with the narrow band neutrino energy, through the quasi-elastic interaction. The physics goal of the first phase is an order of magnitude better precision in the $\nu_\mu \to \nu_\tau$ oscillation measurement ($\delta(\Delta m^2_{23}) = 10^{-4}$ eV^2 and $\delta(\sin^2 2\theta_{23}) = 0.01$), a factor of 20 more sensitive search in the $\nu_\mu \to \nu_e$ appearance ($\sin^2 2\theta_{\mu e} \simeq 0.5 \sin^2 2\theta_{13} > 0.003$), and a confirmation of the $\nu_\mu \to \nu_\tau$ oscillation or discovery of sterile neutrinos by detecting the neutral current events. In the second phase, an upgrade of the accelerator from 0.75 MW to 4 MW in beam power and the construction of 1 Mt Hyper-Kamiokande detector at Kamioka site are envisaged. Another order of magnitude improvement in the $\nu_\mu \to \nu_e$ oscillation sensitivity, a sensitive search of the CP violation in the lepton sector (CP phase δ down to $10^\circ - 20^\circ$), and an order of magnitude improvement in the proton decay sensitivity is also expected.

Contents

1 Introduction

1.1 Physics Motivation

The developments of high-energy physics and astrophysics in twentieth century have finally reached the stage where the universe can be described upto $\sim 10^{-11}$ second after its birth when electro-weak phase transition took place. However, many mysteries remain to be explored. One of the most profound one is the asymmetry of particles and anti-particles in the universe. Another one is the generation problem; i.e. why three generations of quarks and leptons exist, how are their masses and mixing are determined, and whether quarks and leptons are unified at ultra-high energy. All these questions may closely be related, but they are out of scope of the Standard Model of high energy physics. The JHF-Kamioka neutrino project aims at the studies of physics beyond the Standard Model through precision measurements of the masses and mixing of leptons which seem to be very different from those of quarks.

The discovery of the existence of neutrino oscillation in the atmospheric neutrinos by Super-Kamiokande [1] has opened the possibility of detailed studies of the masses and mixing in the lepton sector. The first accelerator-based long baseline neutrino oscillation experiment, K2K, has started [2]. Its first result already show the indication of the oscillation. The establishment of neutrino oscillation in the first generation experiment should be followed by high precision measurements of neutrino oscillation with much more powerful accelerator.

1.2 Neutrino Oscillation

The lepton mixing is described by a unitary 3x3 matrix (Maki-Nakagawa-Sakata [3] (MNS) matrix) that is defined by a product of three rotation matrices with three angles (θ_{12}, θ_{23}, and θ_{13}) and complex phase (δ) as in Cabibbo-Kobayashi-Maskawa matrix [4].

$$\begin{pmatrix} \nu_e \\ \nu_\mu \\ \nu_\tau \end{pmatrix} = \begin{bmatrix} U_{\alpha i} \end{bmatrix} \begin{pmatrix} \nu_1 \\ \nu_2 \\ \nu_3 \end{pmatrix}, \tag{1}$$

$$U = \begin{pmatrix} 1 & 0 & 0 \\ 0 & C_{23} & S_{23} \\ 0 & -S_{23} & C_{23} \end{pmatrix} \begin{pmatrix} C_{13} & 0 & S_{13}e^{-i\delta} \\ 0 & 1 & 0 \\ -S_{13}e^{i\delta} & 0 & C_{13} \end{pmatrix} \begin{pmatrix} C_{12} & S_{12} & 0 \\ -S_{12} & C_{12} & 0 \\ 0 & 0 & 1 \end{pmatrix}, \tag{2}$$

where $\alpha = e,\ \mu,\ \tau$ are the flavor indices, i=1, 2, 3 are the indices of the mass eigenstates, S_{ij} (C_{ij}) stands for $\sin\theta_{ij}$ ($\cos\theta_{ij}$). Neutrinos are produced as flavor eigenstates and each component of mass eigenstates gets a different phase after traveling a certain distance. The detection of neutrino by charged current interactions projects these new state back

onto flavor eigenstates. The probability of oscillation is given by the formula,

$$P(\nu_\alpha \to \nu_\beta) = \delta_{\alpha\beta} \quad - \quad 4\sum_{i>j} \mathrm{Re}(U^*_{\alpha i}U_{\beta i}U_{\alpha j}U^*_{\beta j}) \cdot \sin^2\Phi_{ij} \\ \pm \quad 2\sum_{i>j} \mathrm{Im}(U^*_{\alpha i}U_{\beta i}U_{\alpha j}U^*_{\beta j}) \cdot \sin 2\Phi_{ij} \tag{3}$$

where

$$\Phi_{ij} \equiv \Delta m^2_{ij} L/4E_\nu = 1.27\Delta m^2_{ij}[\mathrm{eV}^2]L[\mathrm{km}]/E_\nu[\mathrm{GeV}], \tag{4}$$

$\Delta m^2_{ij} = m^2_j - m^2_i$, L is the flight distance, and E_ν is the neutrino energy. The $\pm$ sign in the third term is the CP violation effect, $-$ for neutrinos and $+$ for anti-neutrinos. Because $\Delta m^2_{12} + \Delta m^2_{23} + \Delta m^2_{31} = 0$, there exist only two independent Δm^2 for three species of neutrinos. Thus 3 generation neutrino oscillation can be described by two Δm^2's, three angles $(\theta_{12}, \theta_{23}, \theta_{13})$ and one phase (δ).

We take the two Δm^2 values as the values suggested by solar and atmospheric neutrino measurements; $\Delta m^2_{12} \equiv \Delta m^2_{\mathrm{sol}} \simeq 10^{-4} \to 10^{-10}$ eV^2 and $\Delta m^2_{23} \simeq \Delta m^2_{31} \equiv \Delta m^2_{\mathrm{atm}} = (1.6 \sim 4) \times 10^{-3}$ eV^2. For an oscillation measurement with $E_\nu \simeq \Delta m^2_{23} \cdot L$ as in this proposed experiment, the contribution of Δm^2_{12} term is small and the oscillation probabilities can be approximately expressed by two mixing angles;

$$P(\nu_\mu \to \nu_e) = \quad \sin^2 2\theta_{13} \cdot \sin^2\theta_{23} \cdot \sin^2\Phi_{23}, \tag{5}$$

$$P(\nu_\mu \to \nu_\mu) = 1 - \sin^2 2\theta_{23} \cdot \cos^4\theta_{13} \cdot \sin^2\Phi_{23} - P(\nu_\mu \to \nu_e), \tag{6}$$

$$P(\nu_e \to \nu_e) = 1 - \quad \sin^2 2\theta_{13} \quad \cdot \quad \sin^2\Phi_{23}. \tag{7}$$

If we define effective mixing angles as $\sin^2 2\theta_{\mu e} \equiv \sin^2 2\theta_{13} \cdot \sin^2\theta_{23}$ and $\sin^2 2\theta_{\mu\tau} \equiv \sin^2 2\theta_{23} \cdot \cos^4\theta_{13}$, then the expressions reduce to the ones in the two flavor approximation;

$$P(\nu_\mu \to \nu_e) = \quad \sin^2 2\theta_{\mu e} \cdot \sin^2\Phi_{23}, \tag{8}$$

$$P(\nu_\mu \to \nu_\mu) = 1 - \sin^2 2\theta_{\mu\tau} \cdot \sin^2\Phi_{23} - P(\nu_\mu \to \nu_e). \tag{9}$$

Experimental constraints obtained from ν_μ disappearance in the atmospheric neutrino are $\sin^2 2\theta_{\mu\tau} > 0.89$ and $1.6\times10^{-3} < \Delta m^2_{23} < 4\times10^{-3}$ eV^2 [5]. Solar neutrino observations allow several allowed regions in oscillation parameter space. But even for the largest $\Delta m^2_{\mathrm{sol}}$ solution (Large mixing angle solution: LMA), $\Delta m^2_{\mathrm{sol}} \lesssim 1.6 \times 10^{-4}$ eV^2 at 95% CL [6]. The most stringent constraint on θ_{13} comes from reactor $\bar{\nu}_e$ disappearance experiments. As can be seen in eq. (7), $\bar{\nu}_e$ disappearance directly measures θ_{13}. The current limit is $\sin^2 2\theta_{13} < 0.05$ for $\Delta m^2_{23} \simeq 6 \times 10^{-3}$ eV^2 and $\sin^2 2\theta_{13} \lesssim 0.12$ for $\Delta m^2_{23} \simeq 3 \times 10^{-3}$ eV^2 at 90 % C.L [7]. Since θ_{13} is very small and atmospheric neutrino data indicates almost full mixing $\theta_{23} \simeq \pi/4$, the effective two flavor mixing angles defined above and 3 flavor angles have following approximate relations;

$$\sin^2 2\theta_{\mu\tau} \simeq \sin^2 2\theta_{23}, \qquad \sin^2 2\theta_{\mu e} \simeq \frac{1}{2}\sin^2 2\theta_{13} \simeq 2\left|U_{e3}\right|^2. \tag{10}$$

It follows from eq. (3) that CP violation can be observed only with appearance experiments, since $\mathrm{Im}(U^*_{\alpha i}U_{\beta i}U_{\alpha j}U^*_{\beta j}) = 0$ for $\alpha = \beta$. Especially $\nu_\mu \leftrightarrow \nu_e$ oscillation is known to provide the best chance in measuring the CP asymmetry in lepton sector. This is because the leading CP conserving term of $\nu_\mu \leftrightarrow \nu_e$ oscillation is highly suppressed due to small Δm^2_{12} and the subleading terms, such as U_{e3} related and CP violating terms, give leading contributions, as shown below. If the oscillation $\nu_\mu \to \nu_e$ is at the observable level in the first phase of the project, further investigation of CP violation will be carried out in the second phase. In addition since CP violation in three generations requires that all three members should be involved in the process, solar neutrino related quantities (θ_{12}, Δ_{12}) must be large (namely large mixing angle solution for solar neutrino oscillation) in order for the CP violation of the neutrino oscillation to be observable.

The $\nu_\mu \to \nu_e$ appearance probability can be written using MNS matrix element as [8]

$$\begin{aligned} P(\nu_\mu \to \nu_e) =& 4C^2_{13}S^2_{13}S^2_{23}\sin^2\Phi_{31} \\ &+8C^2_{13}S_{12}S_{13}S_{23}(C_{12}C_{23}\cos\delta - S_{12}S_{13}S_{23})\cos\Phi_{32}\cdot\sin\Phi_{31}\cdot\sin\Phi_{21} \\ &-8C^2_{13}C_{12}C_{23}S_{12}S_{13}S_{23}\sin\delta\sin\Phi_{32}\cdot\sin\Phi_{31}\cdot\sin\Phi_{21} \\ &+4S^2_{12}C^2_{13}\left(C^2_{12}C^2_{23} + S^2_{12}S^2_{23}S^2_{13} - 2C_{12}C_{23}S_{12}S_{23}S_{13}\cos\delta\right)\sin^2\Phi_{21} \\ &-8C^2_{13}S^2_{13}S^2_{23}\left(1-2S^2_{13}\right)\frac{aL}{4E_\nu}\cos\Phi_{32}\sin\Phi_{31}. \end{aligned} \tag{11}$$

The first term has the largest contribution. The second $\cos\delta$ term is generated by CP phase δ but CP conserving. The third $\sin\delta$ term violates CP. The fourth term, which is the solar neutrino term, is suppressed by $\sin^2\frac{\Delta m^2_{21}L}{4E_\nu}$. The matter effect is characterized by

$$a = 2\sqrt{2}G_F n_e E_\nu = 7.6\times10^{-5}\rho[\mathrm{g/cm^3}]E_\nu[\mathrm{GeV}] \qquad [\mathrm{eV^2}], \tag{12}$$

where G_F is the Fermi constant, n_e is the electron density and ρ is the earth density. The probability $P(\bar\nu_\mu \to \bar\nu_e)$ is obtained by the replacing $a \to -a$ and $\delta \to -\delta$ in eq. (11). As seen in eq. (12) the matter effect is proportional to neutrino energy, so the lower the energy, the smaller the effect is. The CP asymmetry in the absence of matter effect is calculated as

$$A_{CP} = \frac{P(\nu_\mu \to \nu_e) - P(\bar\nu_\mu \to \bar\nu_e)}{P(\nu_\mu \to \nu_e) + P(\bar\nu_\mu \to \bar\nu_e)} \simeq \frac{\Delta m^2_{12}L}{4E_\nu}\cdot\frac{\sin2\theta_{12}}{\sin\theta_{13}}\cdot\sin\delta \tag{13}$$

Because θ_{13} is small, CP asymmetry can be large, especially for small E_ν.

2 Overview of the experiment

The JHF-Kamioka neutrino project is a long baseline neutrino oscillation experiment using the JHF 50 GeV proton synchrotron (PS). The JHF project was officially approved in 2001 by the Japanese government. The construction of the 50 GeV PS will be completed in 2006. The 50 GeV PS is designed to deliver 3.3×10^{14} protons every 3.4 seconds

(0.77 MW), later to be upgraded to 4 MW [9]. A high intensity narrow-band neutrino beam of energy around 1 GeV is produced by using the full proton intensity. The initial far detector is Super-Kamiokande, a 50 kt water Čerenkov detector. The baseline length of the experiment for neutrino oscillation is 295 km between JHF at Tokai and Super-Kamiokande at Kamioka as shown in Figure 1. A 1 Mt Water Čerenkov detector,

Figure 1: Baseline of the JHF-Kamioka neutrino project

Hyper-Kamiokande to be built at Kamioka, is proposed as the second far detector.

A feature of the JHF-Kamioka neutrino experiment is its high intensity narrow band neutrino beam. The neutrino energy of narrow band beam is tunable, and the well-defined energy spectrum has an advantage to achieve the maximum sensitivity for neutrino oscillation. The peak of the beam energy will be tuned at the point of maximum oscillation and the width will be narrowed to suppress the background from non-oscillated neutrinos. With 295 km baseline, the neutrino energy will be tuned to between 0.4 and 1.0 GeV, which corresponds to Δm^2 between 1.6×10^{-3} and 4×10^{-3} eV^2 suggested by the recent Super-Kamiokande result [5]. In the design of the neutrino beam line, a shorter decay volume is adopted to lower the ν_e flux from muon decays, which is an intrinsic background in $\nu_\mu \rightarrow \nu_e$ search. The narrow band neutrino beam is produced with a conventional method in which parent pions are focused by two magnetic horns. There are two methods to make the narrow band beam: one is momentum-selection of the parent pions by a dipole magnet and the other is a technique called off-axis tuning described in Section 3.

Another feature of the experiment is the reconstruction of the neutrino energy using quasi-elastic (QE) interaction. The QE interaction is the dominant process at a neutrino energy around 1 GeV. In QE interaction, the neutrino energy can be well reconstructed with the charged lepton in charged current interaction. In QE interaction, the neutrino

energy is expressed as:

$$E_\nu = \frac{m_N E_l - m_l^2/2}{m_N - E_l + p_l cos\theta_l}, \tag{14}$$

where m_N and m_l is the mass of the neutron and the lepton (=e or μ), and E_l, p_l and θ_l is the energy, the momentum, and the angle of the lepton relative to the neutrino beam, respectively. This method matches well with the characteristics of the water Čerenkov detector which has an excellent performance for electrons, muons and photons in this energy scale. As an example, the relation between the reconstructed neutrino energy and the true one, and the energy resolution of ν_μ events are shown in Figure 2 for 2 degree off-axis beam explained in Section 3.

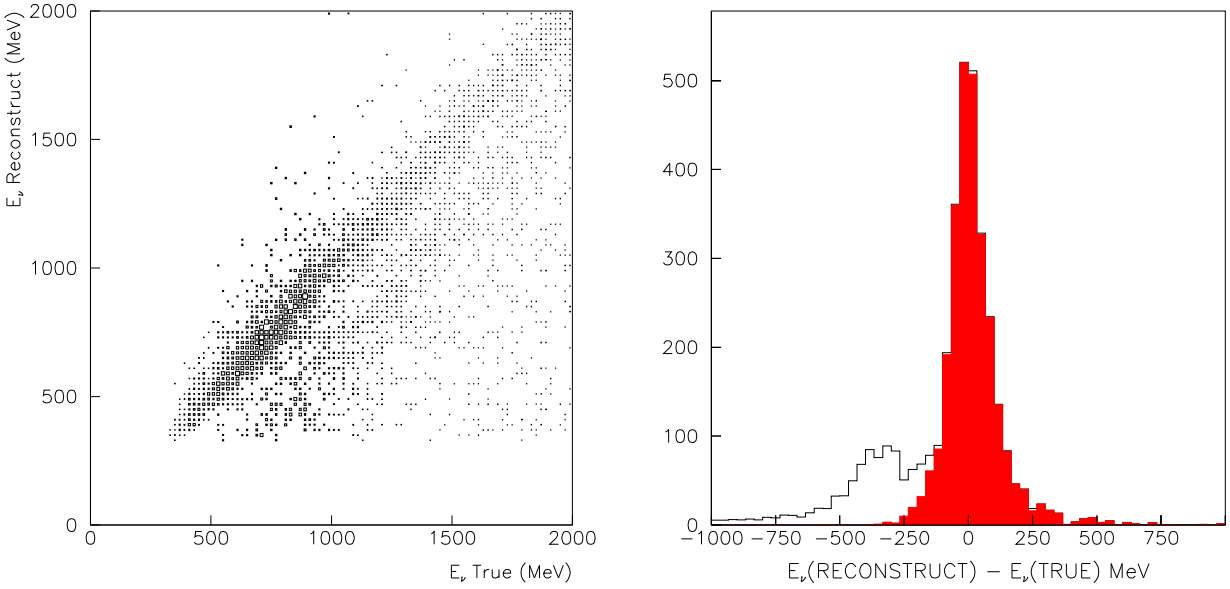

Figure 2: (left) The scatter plots of the reconstructed neutrino energy versus the true one for ν_μ events. The method of the energy reconstruction is expressed in Equation 14. (right) The energy resolution of ν_μ events for 2 degree off-axis beam. The shaded (red) histogram is for the true QE events.

The project is divided into two phases. In the first phase, the main physics goal is the precision measurement of neutrino oscillation with the 50 GeV PS of 0.77 MW beam power and Super-Kamiokande. Typically, 5,000 ν_μ interactions per year in the full volume of the detector are expected without neutrino oscillation. In $\nu_\mu \to \nu_\mu$ oscillation channel, a measurement of the oscillation pattern determines $\sin^2 2\theta_{23}$ with 1% precision and Δm^2 with a precision better than 10^{-4} eV^2. A non-oscillation scenario, such as a model of neutrino decay or a model with extra dimension [10], can be ruled out in the measurement. A search for $\nu_\mu \to \nu_e$ appearance channel is conducted with a sensitivity of $\sin^2 2\theta_{\mu e} (\equiv 0.5 \sin^2 2\theta_{13})$ down to 0.003 (90%C.L.). Many theories suggest large value of $\sin^2 2\theta_{\mu e}$ [11]. A confirmation of $\nu_\mu \to \nu_\tau$ oscillation is carried out by counting the number of neutral current interaction. The measurement also constrains the existence of a sterile neutrino or a model of non-oscillation, which is introduced to explain both

LSND result and solar neutrino results together with atmospheric neutrino oscillation. In the second phase, there are mainly three physics goals: (1) search for $\sin^2 2\theta_{e\mu}$ below 5×10^{-4} level, (2) search for CP violation in neutrino oscillation, and (3) discovery of the proton decay as an evidence of the Grand unification theory (GUT). In the search for CP violation, the low energy neutrino beam has the advantage of large CP asymmetry and small matter effect as discussed in Section 1.2.

The JHF-Kamioka neutrino project is a unique experiment in the world. The experiment has much more sensitivity for neutrino oscillation than other long baseline neutrino experiments (K2K, MINOS, and OPERA) due to the high power JHF accelerator and the huge Super-Kamiokande detector. The second phase of the experiment is competitive with a recent proposal of a neutrino factory [12] in terms of CP violation reach and uses established technologies. The JHF-Kamioka neutrino project is expected to start in 2007 at the same time of completion of the JHF accelerator.

3 Neutrino beam at JHF

The layout of JHF facility is drawn in Figure 3. The proton beam is fast-extracted

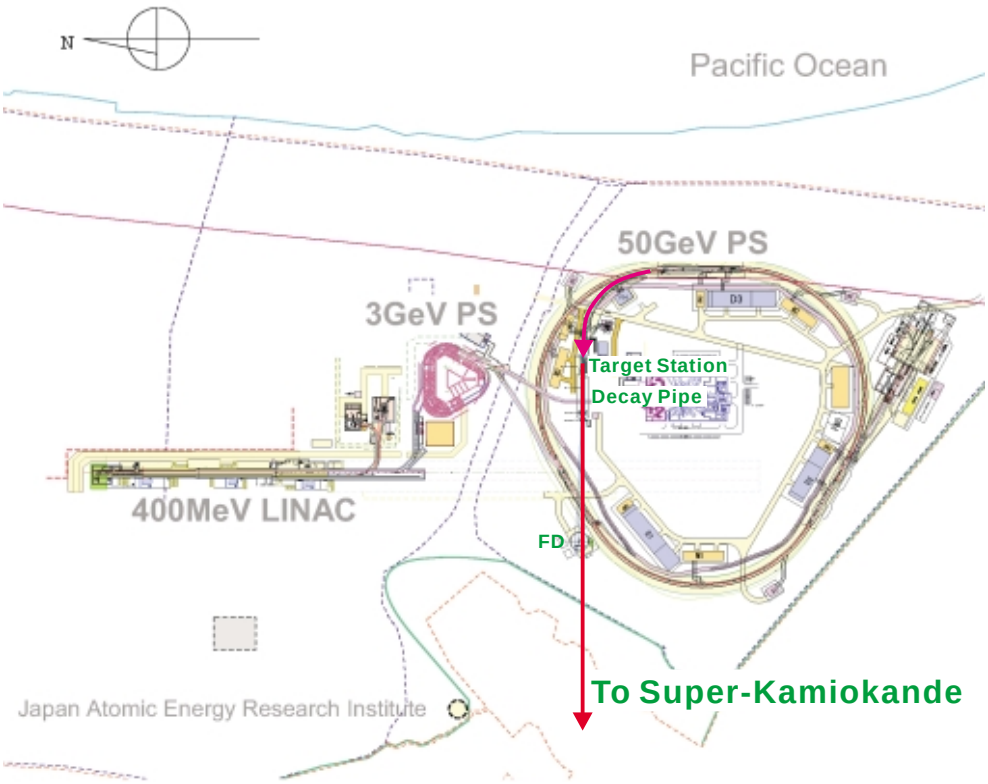

Figure 3: Layout of JHF.

from the 50 GeV PS in a single turn and transported to the production target. The design intensity of the PS is 3.3×10^{14} protons/pulse (ppp) at a repetition rate of 0.292 Hz (3.42 second period), resulting in a beam power of 0.77 MW (2.64 MJ/pulse). The spill width is $\sim$5.2 μsec. We define a typical one year operation as 10^{21} protons on target

(POT), which corresponds to about 130 days of operation. The protons are extracted toward inside of the PS ring, and are bent by 90° to SK direction by the transport line with a radius of curvature of 110 m smaller than the PS arc. We will adopt superconducting magnets for the transport line. The secondary pions (and kaons) from the target are focused by electromagnetic horns [13], and decay in the decay pipe. The length of the decay pipe from the target position is 80 m. The first front detector is located at 280 m from the target.

There are three options of beam configurations; wide band beam (WBB), narrow band beam (NBB) and off axis beam (OAB). The difference is in the optics for the secondary particles. The WBB uses two electromagnetic horns to focus secondary pions. Horn-focused WBB has been widely used in experiments including K2K. Since the momentum and angular acceptance of the horn system is large, the resulting neutrino spectrum becomes wide. The NBB is obtained by placing a dipole magnet between the two horns of WBB. Momentum selected pion beam produces a monochromatic neutrino beam. The peak neutrino energy can be tuned easily by changing the current of the dipole magnet. The OAB is another option to produce a narrow neutrino energy spectrum [14]. The optics is almost same as the WBB, but the axis of the beam optics is displaced by a few degree from the far detector direction (off-axis). With a finite decay angle, the neutrino energy becomes almost independent of parent pion momentum as a characteristics of the Lorenz boost, which provides the narrow spectrum. The peak neutrino energy can be adjusted by choosing the off-axis angle. For each of the above beam configurations, ν_μ and $\bar{\nu}_\mu$ can be switched by flipping the polarity of the focusing magnets.

Monte-Carlo (MC) simulations using GEANT [15] have been performed to estimate expected neutrino spectra and number of events. The target, horns, bending magnet and decay pipe are put into the geometry of the simulation. The target is assumed to be simple Cu rod of 1-cm diameter and 30-cm long. Hereafter we refer to the NBB with selected pion momentum of # GeV/c as LE#π and OAB with a beam axis # degree offset as OA#°. The simulation code is essentially the one used in the K2K experiment except for the hadron production model. The Calor-Fluka model [16], which is known to work better at higher energies, is used in the present simulation while a dedicated model base on hadron production data taken near 12 GeV is used in the K2K. From the observation of neutrino events at front detector of K2K, the K2K beam MC is known to provide absolute neutrino flux within 20% error.

Fig. 4 shows expected neutrino energy spectrum of charged current interactions at Super-Kamiokande. Fluxes and numbers of interactions are summarized in Table 1. LE2π and OA2° have a sharp peak at ∼0.95 GeV and ∼0.7 GeV, respectively, and WBB has a broad peak at ∼1 GeV. The OAB is roughly a factor of three more intense than NBB. NBB has the least high energy tail among the three beams. The ν_e contamination in the beam are expected to be 0.7%, 0.7% and 1.0% for WBB, LE2π and OA2°. The sources of ν_e are $\pi \to \mu \to e$ decay chain and K decay (K_{e3}). Their fractions are μ-dacay: 54%, K-decay: 46% for LE2π and μ-dacay: 37%, K-decay: 63% for OA2°. The energy spectra of the ν_e contamination are plotted in Fig. 5. At the peak energy of ν_μ spectrum, the ν_μ/ν_e ratio is as small as 0.2% in the cases of NBB and OAB. This indicates that

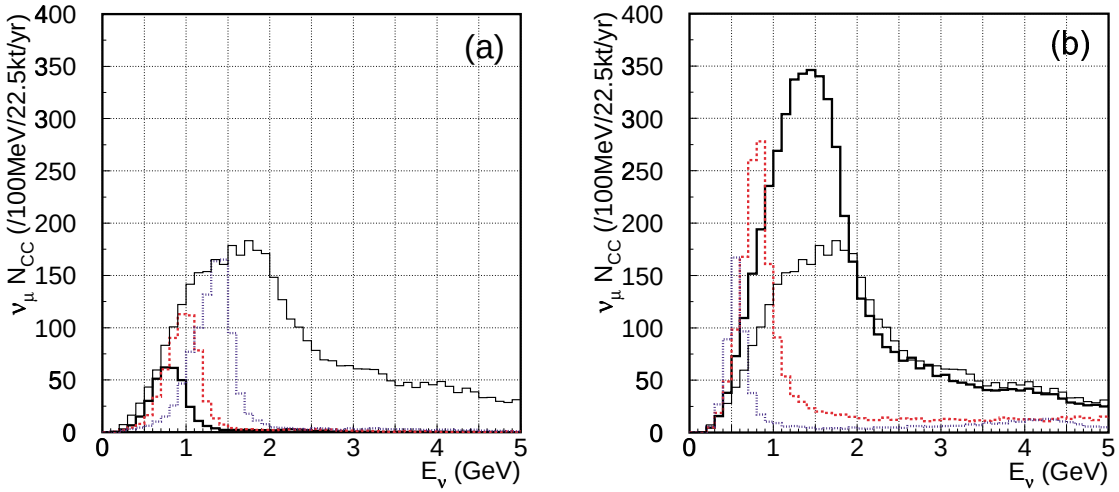

Figure 4: Neutrino energy spectra of charged current interactions. Thick solid, dashed and dotted histograms in (a) are LE1.5π, LE2π and LE3π, and those in (b) are OA1°, OA2° and OA3°, respectively. WBB is drawn by thin solid histogram in both (a) and (b).

Table 1: Summary of ν_μ beam simulation. The peak energy $E_{\rm peak}$ is in GeV. The flux is given in $10^6/{\rm cm}^2/{\rm yr}$, and the ν_e/ν_μ flux ratio is in %. The ratio in the "total" column is the one integrated over neutrino energy and the column "$E_{\rm peak}$" is the ratio at the peak energy of ν_μ spectrum. The normalization for the number of interactions are /22.5kt/yr. The numbers outside (inside) the bracket are number of total (CC) interactions.

		Flux		ν_e/ν_μ(%)		# of interactions	
Beam	$E_{\rm peak}$	ν_μ	ν_e	total	$E_{\rm peak}$	ν_μ	ν_e
WIDE	1.1	25.5	0.19	0.74	0.34	7000(5200)	78(59)
LE1.5π	0.7	5.3	0.05	1.00	0.39	510(360)	5.7(4.2)
LE2π	0.95	7.0	0.05	0.73	0.15	870(620)	6.8(5.0)
LE3π	1.4	8.0	0.05	0.65	0.16	1400(1000)	9.3(6.9)
OA2°	0.7	19.2	0.19	1.00	0.21	3100(2200)	60(45)
OA3°	0.55	10.6	0.13	1.21	0.20	1100(800)	29(22)

beam ν_e background is greatly suppressed (factor ~ 4) by appling energy window cut in the event selection. The μ decay is the largest contribution at the peak neutrino energy as shown in the figure.

One of the sources of systematic uncertainties in estimating the expected number of events in the far detector from the observation in the near detector is the spectrum difference between far site and near site. In Figure 6, spectra at far and near sites are compared. The peak postion is shifted to higher energy at the far site than at the near site. The far/near spectrum ratio is also plotted in the figure. The difference is as large as 40$\sim$50% for NBB and OAB and reaches almost 80% for WBB. The sources of this far/near difference are

- Difference in the solid angle between far and near detectors. Larger angle neutrinos from beam axis can contribute more to the near detector than to the far detector.

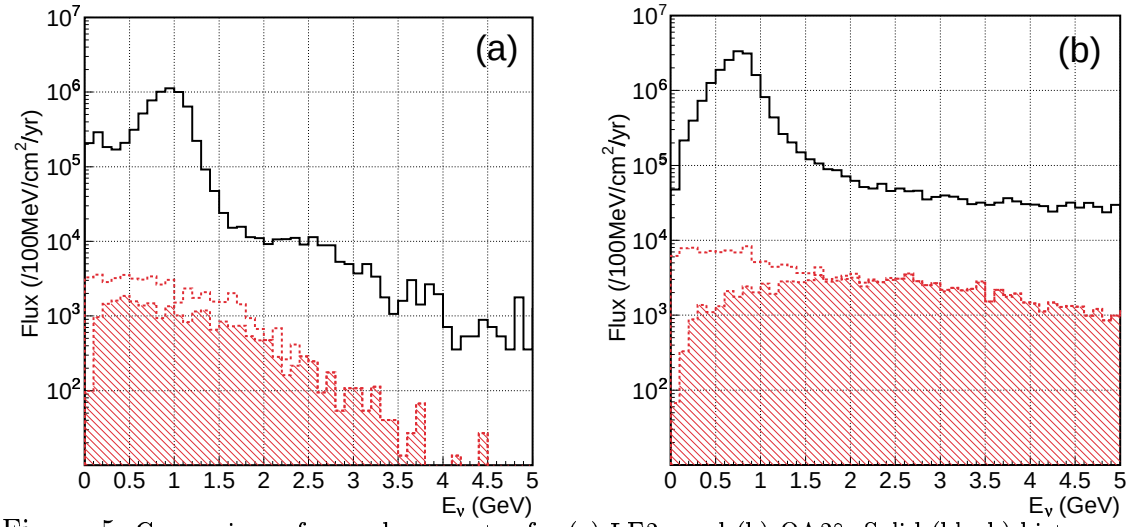

Figure 5: Comparison of ν_e and ν_μ spectra for (a) LE2π and (b) OA2°. Solid (black) histogram is ν_μ and dashed (red) one is ν_e. Hatched area is contribution from K decay.

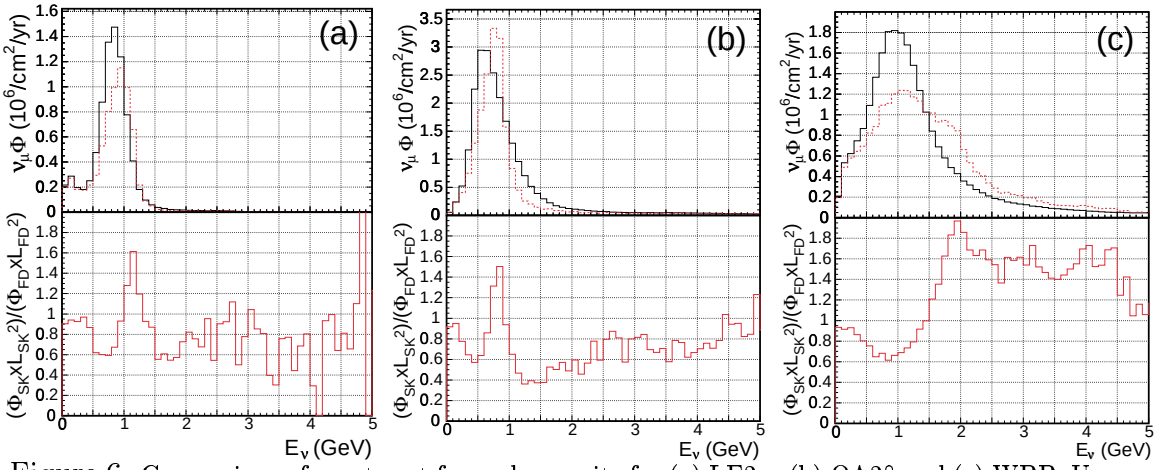

Figure 6: Comparison of spectra at far and near site for (a) LE2π, (b) OA2° and (c) WBB. Upper figure is ν_μ spectra at 280 m (solid black histogram) and 295 km (dashed red histogram). The flux for the near site is multiplied by $(295/0.28)^2$ to directly compare the spectra. The front detector size is assumed to be ± 5 m in horizontal and vertical directions. The lower plots are far/near ratio of fluxes.

The Large angle neutrinos have different energies from neutrinos at zero degree direction.

- Finite length of decay pipe. The near detector has a larger solid angle for pions which decay near the end of the decay pipe than those decaying at the beginning of the decay pipe. Higher momentum pions decay further downstream. For the far detector, the length of the decay pipe can be neglected as a point source. Thus the neutrino spectrum is also distorted by this finite decay pipe effect.

At the distance longer than one km from the target, both of the above two effects become negligible and the far/near ratio becomes flat.

4 Secondary beam monitor and Neutrino detectors

4.1 Muon monitor

Muons from pion decays are measured by the muon monitor. Only such a beam monitor can monitor the beam condition spill by spill, since a neutrino detector cannot monitor the beam condition in such a short period of spill. The primary purpose of the muon monitor is to measure the beam direction with a precision of 1 mrad similar to K2K [2] by measuring the center of the muon beam profile. The stability of the neutrino beam intensity is also monitored by measuring the time dependent muon yield.

The beam monitor is located right after the beam dump which stops all hadronic activities. We prepare separate beam monitors for each beam, since the beam center and the muon energy of NBB is different from those of OAB.

4.2 Near neutrino detector

The main purposes of the front-detector at the near site are as follows.

1. Measurement of the neutrino flux to estimate the flux at SK.
2. Measurement of the neutrino energy spectrum. The spectrum measurement as a function of the distance from the beam center gives constraint on the estimation of the "far/near" ratio.
3. Measurement of neutrino cross sections for various interaction modes, such as charged current quasi-elastic, charged current non quasi-elastic, and neutral current interactions.
4. Measurement of the ν_e contamination for the ν_e appearance search.
5. Measurement and monitoring of neutrino beam direction.

For these purposes, we have several options for the detector. For low energy neutrinos with energy below 1 GeV, fully active detectors, such as water Čerenkov and a fine grained scintillator detectors satisfy our requirements. Because typical event rate in the first near detector is 0.06 events per spill per ton for OAB and $\sim$ 0.02 events for NBB, it hard to use a water Čerenkov detector like the 1kt detector of K2K. The fully active scintillator tracker proposed for the K2K upgrade [17] can be operated at high event rate. The difference in the neutrino target material between H_2O and CH_2 needs to be studied using the near detector and the narrow-band neutrino beam.

There is a possibility of a second near detector located at a few kilometers distance from the target. At that distance, the "far/near ratio" is almost flat as discussed in section 3. In addition, because the neutrino flux is not as high as at the near site, a Water Čerenkov detector can be operated with a reasonable event rate. Currently, we look for a place for the detector, and we study the necessity of the detector at the position.

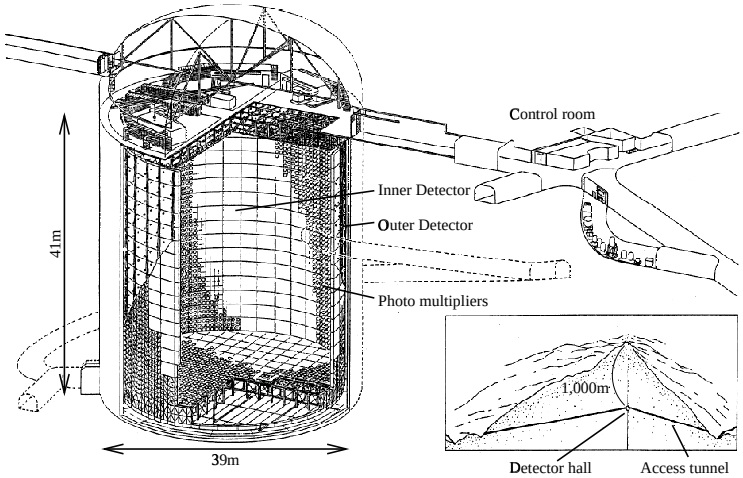

Figure 7: A schematic view of the Super-Kamiokande Detector.

4.3 Far detector: Super-Kamiokande

The far detector, Super-Kamiokande, is located in the Kamioka Observatory, Institute for Cosmic Ray Research (ICRR), University of Tokyo, which has been successfully taking data since 1996. The detector is also used as a far detector for K2K experiment. It is a 50,000 ton water Čerenkov detector located at a depth of 2,700 meters water equivalent in the Kamioka mine in Japan. Its performance and results in atmospheric neutrinos or solar neutrinos have been well documented elsewhere[1, 5, 6]. A schematic view of detector is shown as Fig 7. The detector cavity is 42 m in height and 39 m in diameter, filled with 50,000 tons of pure water. There is an inner detector (ID), 33.8 m diameter and 36.2 m high, surrounded by an outer detector (OD) of approximately 2 m thick. The inner detector has 11,146 50 cm ϕ photomultiplier tubes (PMTs), instrumented on all surfaces of the inner detector on a 70.7 cm grid spacing. The outer detector is instrumented with 1,885 20 cm ϕ PMTs and used as an anti-counter to identify entering/exiting particles to/from ID. The fiducial volume is defined as 2 m away from the ID wall, and the total fiducial mass is 22,500 ton. Čerenkov rings produced by relativistic charged particles are detected by ID PMT's. The trigger threshold is recently achieved to be 4.3 MeV. The pulse hight and timing information of the PMT's are fitted to reconstruct the vertex, direction, energy, and particle identification of the Čerenkov rings. A typical vertex, angular and energy resolution for a 1 GeV μ is 30 cm, 3° and 3% for vertex, respectively. The Čerenkov ring shapes, clear ring for muons and fuzzy ring for electrons, provides good e/μ identification. A typical rejection factor to separate μ's from e's (or vice versa) is about 100 for a single Čerenkov ring events at 1 GeV. The e's and μ's are further separated by detecting decay electrons from the μ decays. A typical detection efficiency of decay electrons from cosmic stopping muons is roughly 80% which can be improved by further analysis. A 4π coverage around the interaction vertex provides an efficient π^0 detection and e/π^0 separation as discussed in sections 5.2 amd 5.3.

Interactions of neutrinos from the accelerator are identified by synchronizing the tim-

ing between the beam extraction time at the accelerator and the trigger time at Super-Kamiokande using the the Global Positioning System (GPS). The synchronization accuracy of the two sites is demonstrated to be less than 200 ns in the K2K experiment. Because of this stringent time constraint, and the quiet environment of the deep Kamioka mine, chance coincidence of any entering background is negligibly low. A typical chance coincidence rate of atmospheric neutrino events is 10^{-10}/spill, which is much smaller than the signal rate of about 3×10^{-3}/spill for the WBB option.

5 Physics in the first stage of the project

5.1 High precision measurement of Δm_{23} and θ_{23} with ν_μ disappearance

The neutrino energy can be reconstructed through quasi-elastic (QE) interactions as shown in Equation 14 by the Super-Kamiokande (SK) detector. In this analysis, we use the same muon selection criteria as those used in the atmospheric neutrino analysis by the Super Kamiokande collaboration [1]; fully contained single ring muon-like events in a fiducial volume of 22.5 kt. The neutrino energy spectrum at SK in five years exposure of the JHF OA2° neutrino beam is shown in Figure 8 (bottom) assuming no neutrino oscillation. The observed energy spectrum for the neutrino oscillation with the parameters of $(\Delta m_{23}, \theta_{23}) = (3 \times 10^{-3}\mathrm{eV}^2, \pi/4)$ is shown in Figure 8 (top), which shows large dip at around 800 MeV. In this analysis, θ_{13} is approximated to be zero and thus $\sin^2 2\theta_{\mu e} = \sin^2 2\theta_{23}$. The value of θ_{13} will be determined in the $\nu_\mu \to \nu_e$ search.

In the oscillation analysis, the true neutrino energy spectrum is extracted by subtracting the contribution of non-QE background events. To measure the oscillation parameters, full Super-Kamiokande Monte Carlo events are generated and the ratio between the "measured" spectrum at SK and the the expected one without oscillation is fitted by the function of $P(\nu_\mu \to \nu_\mu)$ in Equation 6 after subtracting the non-QE contribution. Since the spectrum of non-QE events depends on the oscillation parameters, the non-QE spectrum are updated by the fit result at each iteration of the fitting. The survival probability of $P(\nu_\mu \to \nu_\mu)$ is shown in Figure 9, which gives the fit result of $(\Delta m_{23}, \sin^2 2\theta_{23}) = ((2.96 \pm 0.04) \times 10^{-3}\mathrm{eV}^2, 1.0 \pm 0.01)$. The oscillation pattern is clearly seen and the $\sin^2 2\theta_{23}$ precision of 1 % and the Δm_{23} precision of 4×10^{-5} eV^2 are expected.

Several beam configurations are studied in the range of Δm_{23} between 1×10^{-3} and 1×10^{-2} eV^2. The result is summarized in Figure 10. With OA2°, the maximum sensitivity to the oscillation parameters is achieved at $\Delta m_{23} = (3 \sim 3.5) \times 10^{-3}$ eV^2.

So far, we assumed $\sin^2 2\theta_{23} = 1.0$. In the case of $\sin^2 2\theta_{23} = 0.9$, which is the lower bound suggested by atmospheric neutrino result of Super-Kamiokande, is shown in Figure 11. The precision is slightly worse due to non-oscillated neutrino events at the oscillation maximum.

By selecting the bin at the oscillation maximum, the disappearance signal dip is en-

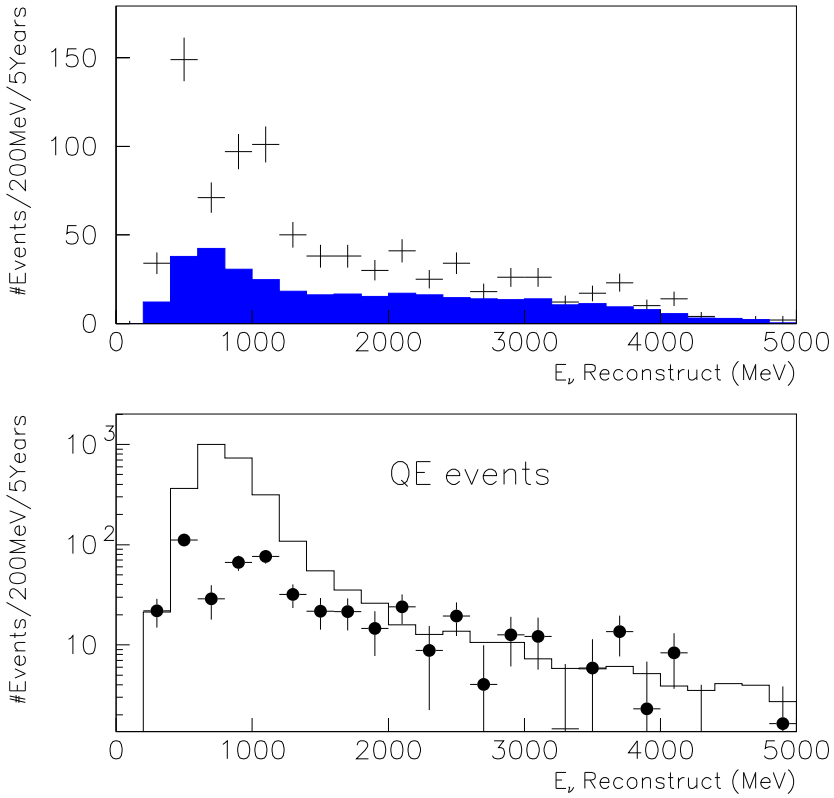

Figure 8: The neutrino energy spectrum measured in SK for 5 years exposure of JHF OA2°. The top plot is in the case of neutrino oscillation with parameters of $(\Delta m_{23}, \theta_{23}) = (3 \times 10^{-3}\ \mathrm{eV}^2, \pi/4)$. The contribution of non-QE interactions is shown by the shaded (blue) histogram. The bottom plot is for QE events after subtracting the non-QE contributions. The dot is the case of the oscillation corresponding to the top plot, and the histogram is in the case of null oscillation. The error bar is from the statistics of 5 years.

hanced and thus the contribution of the systematic uncertainties are largely suppressed. For example, the depth of the dip in Figure 9, which corresponds to $1 - \sin^2 2\theta_{23}$, is as small as 3%. Thus, a systematic uncertainty of 10% in the flux normalization (far/near ratio) contributes to 3% $\times$ 0.1 =0.3% in the $\sin^2 2\theta_{23}$ measurement. Assuming 10% systematic uncertainty in the far/near ratio, which is similar to K2K's number of 6%, 4% uncertainty in the energy scale, and 20% uncertainty in the non-QE background subtraction, the total systematic error is estimated to be less than 1 % for $\sin^2 2\theta_{23}$ and less than 1×10^{-4} eV^2 for Δm_{23}. The systematic uncertainties are expected to be reduced further below the statistical uncertainties by the neutrino flux measurement using QE events and detailed non-QE background measurement by the front detector, by the pion production measurement, and possibly a second near detector at a few km point which makes the systematics in the far/near ratio negligible.

The overall sensitivity of the first phase is expected to be 1% in precision for $\sin^2 2\theta_{23}$ and better than 1×10^{-4} eV^2 for Δm_{23}.

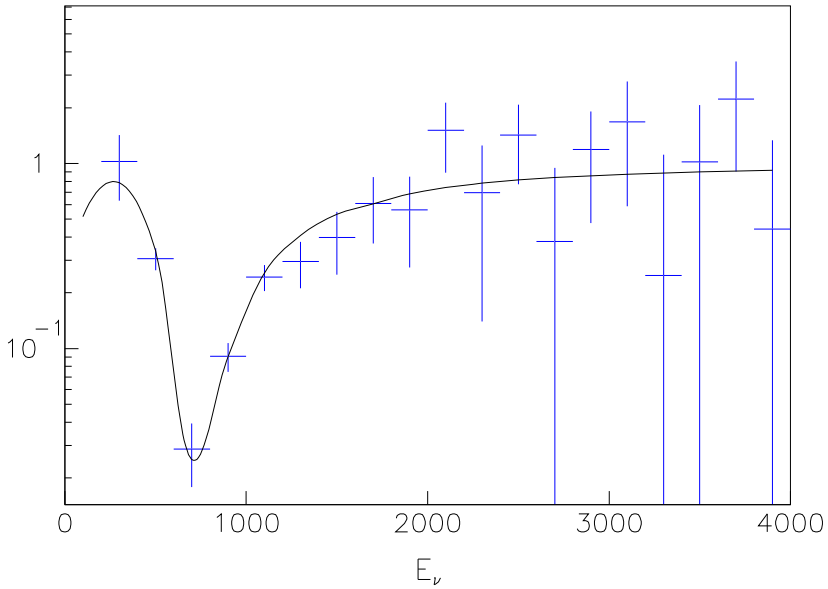

Figure 9: The ratio of the measured spectrum with neutrino oscillation to the expected one without neutrino oscillation after subtracting the contribution of non QE-events. The fit result of the oscillation is overlaid.

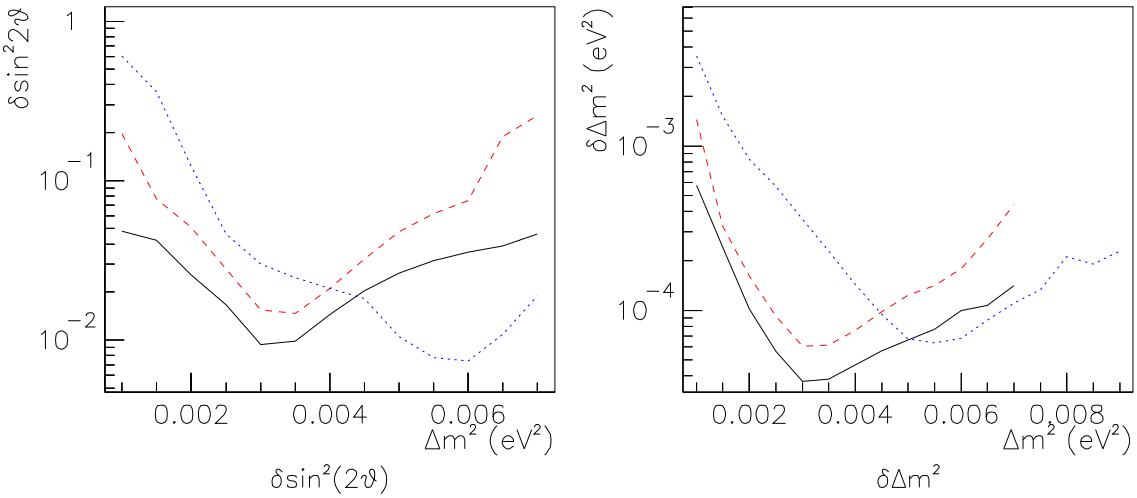

Figure 10: The final sensitivity of the neutrino oscillation parameters: $\sin^2 2\theta_{23}$ (left) and Δm_{23} (right), as a function of true Δm_{23} (eV^2). The $\sin^2 2\theta_{23}$ is set to 1.00. The result with OA2° is shown by the black (solid) line, LE1.5π by the red (dashed) line and LE3π by the blue (dotted) line.

5.2 ν_e appearance search

The JHF neutrino beam has small ν_e contamination (0.2% at the peak energy of OAB and NBB) and the ν_e appearance signal is enhanced by tuning the neutrino energy at its expected oscillation maximum. Reconstruction of the neutrino energy provides

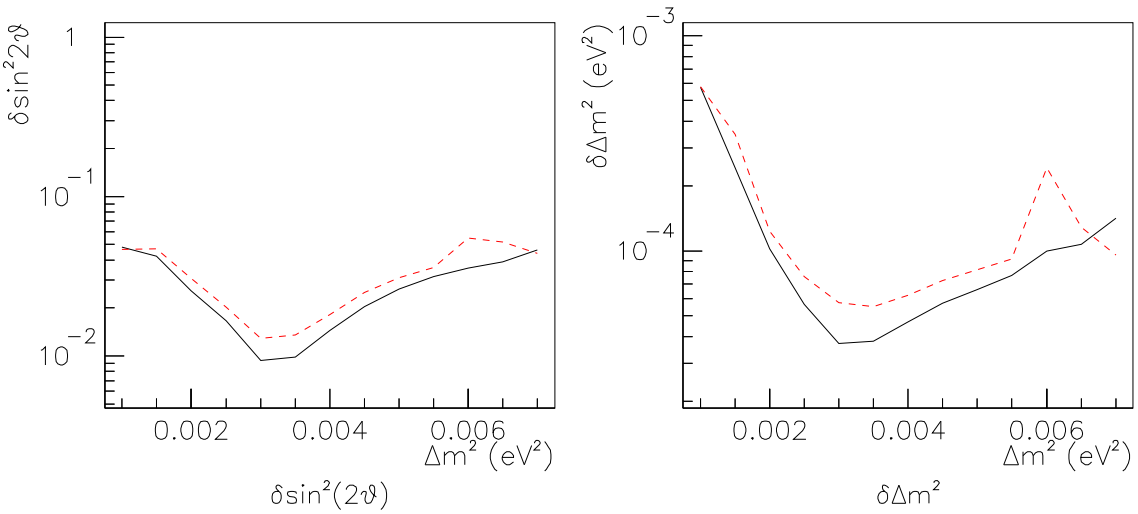

Figure 11: The final sensitivity of the neutrino oscillation parameters in the case of $\sin^2 2\theta_{23} = 0.9$ shown by red (dashed) line: $\sin^2 2\theta_{23}$ (left) and Δm_{23} (right), as a function of true Δm_{23} (eV^2). As a reference, the result of $\sin^2 2\theta_{23} = 1.00$ is shown in black line (solid).

oscillation pattern and makes a positive identification of the ν_e appearance signal. Thus, JHF-Kamioka neutrino experiment has an excellent opportunity to discover ν_e appearance and thus measure θ_{13}. In this section, the sensitivity on ν_e appearance is described based on the full Monte Carlo simulations and analysis of Super-Kamiokande and K2K experiments.

5.2.1 Background sources and event selection criteria

The process of the ν_e appearance signal is searched for in the QE interaction. Since the proton momentum from the QE interaction is usually below the Čerenkov threshold, the signal has only a single electro-magnetic shower (single ring e-like). The possible background processes are $\nu_\mu \to \mu$ with e/μ misidentification, ν_e contamination, and π^0 background. The background from μ misidentification is found to be negligible due to excellent e/μ separation of Super-Kamiokande. The ν_e contamination is as small as 0.2-0.3%. A π^0 produced by neutral current and inelastic charged current processes is a possible background when one of the photon is missed or 2 photons overlaps.

The standard Super-Kamiokande atmospheric neutrino analysis requirements are used to select a single ring e-like event: single ring, electron like (showering), visible energy greater than 100 MeV, and no decay electrons. The electron identification eliminates all of the μ background, and the decay electron cut further eliminates inelastic charged current processes associated with π^0. Reduction of number of events by the "standard" 1ring e-like cut for charged and neutral current events are listed in Table 2 2). The remaining background events at this stage are predominantly from single π^0 production through neutral current interaction and a ν_e contamination.

For neutrino energies below 1 GeV, the energy of produced π^0 is low and thus the

Table 2: Number of events and reduction efficiency of "standard" 1ring e-like cut and π^0 cut for 5 year exposure (5×10^{21} p.o.t.) OA2°. For the calculation of oscillated ν_e,$\Delta m^2 = 3 \times 10^{-3}$ eV^2 and $\sin^2 2\theta_{\mu e} = 0.05$ is assumed.

OAB 2°	ν_μ C.C.	ν_μ N.C.	Beam ν_e	Oscillated ν_e
1) Generated in F.V.	10713.6	4080.3	292.1	301.6
2) 1R e-like	14.3	247.1	68.4	203.7
3) e/π^0 separation	3.5	23.0	21.9	152.2
4) 0.4 GeV$< E_{rec} <$ 1.2 GeV	1.8	9.3	11.1	123.2

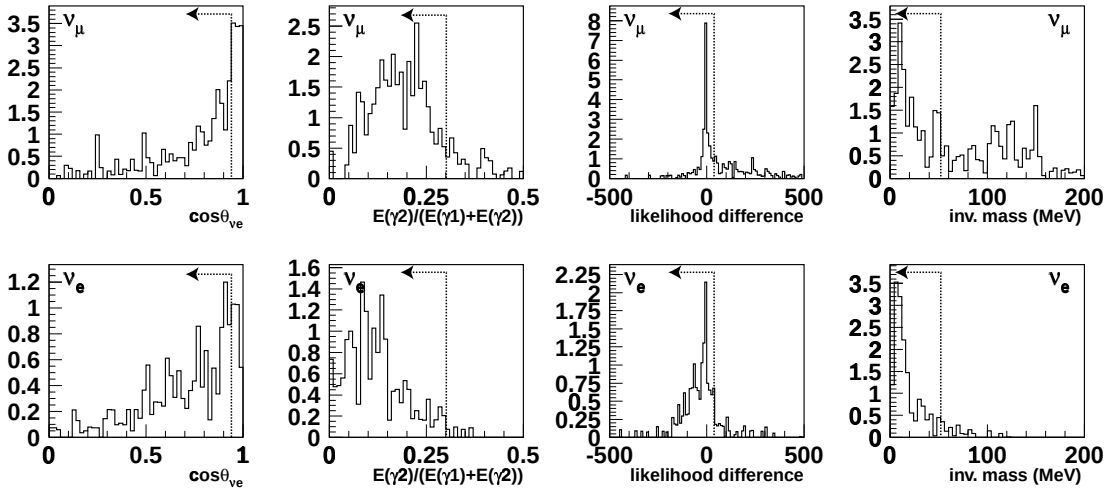

Figure 12: Distributions of the four quantities, used in the e/π^0 separation. The beam is the wide band beam and events are after the single-ring e-like selection. Upper histograms corresponds to ν_μ background events and the lower histograms correspond to the ν_e signal events. The arrows in the figure show the cut positions used in the analysis.

probability of the two photons to merge to one is small. The limitation comes from asymmetric decay of π^0 with one high and one low photon energies, where the lower energy photon tends to be hidden under the scattered light[1] of the higher energy photon. In order to recover this hidden lower energy photon and further suppress the π^0 background, the photomultiplier hit pattern including scattered light is fitted under the hypotheses of single and that of double electro-magnetic rings. Figure 12 shows distributions of four characteristic quantities that separates signal ν_e events from π^0 background events as follows:

- Angle between ν and e ($\cos\theta_{\nu e}$):
  Some fraction of π^0 background has a steep forward peak, which is likely due to coherent π^0 production. Those events in the extreme forward direction are rejected.
- Energy fraction of lower energy ring ($\frac{E(\gamma_2)}{E(\gamma_1)+E(\gamma_2)}$)

[1]About 10-20% of the light are scattered in the water before reaching the photomultiplier tubes causing broadly distributed background light.

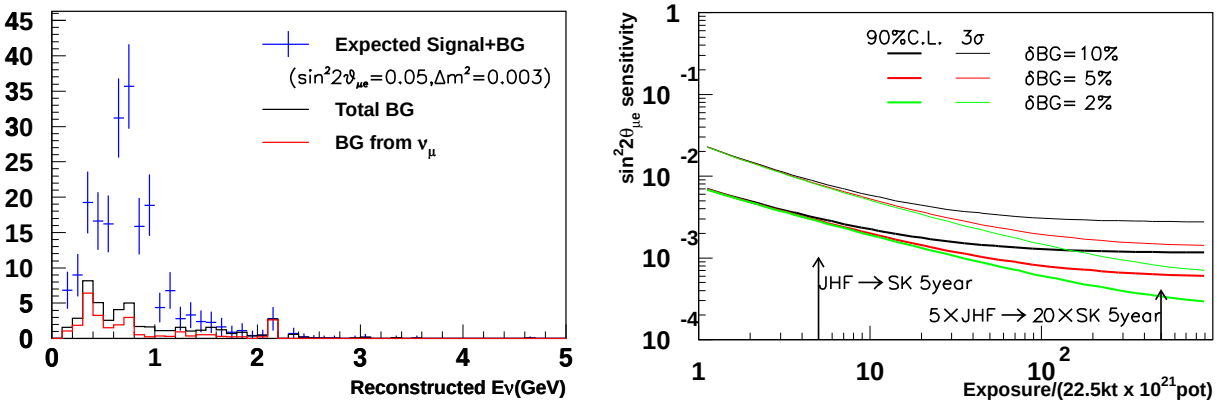

Figure 13: Left:Expected reconstructed neutrino energy distributions of expected signal+BG, total BG, and BG from ν_μ interactions for 5 years exposure of OA2°. Right: Expected (thick lines:) 90%CL sensitivity and (thin lines:) 3σ discovery contours as the functions of exposure time of OA2°. In left figure, expected oscillation signals are calculated with the oscillation parameters: $\Delta m^2 = 3 \times 10^{-3}$ eV^2,sin$^2\,2\theta_{\mu e} = 0.05$. In right figures, Three different contours correspond to 10%, 5%, and 2% uncertainty in the background estimation.

The ν_e signal tends to have a low energy second ring which is either a fake ring or a ring due to bremsstrahlung. Those events with the large energy fraction are rejected.

- Difference between double and single ring likelihood:
  Single ring like events are selected.
- Invariant mass of 2 photons:
  The π^0 background shows a peak at 135 MeV whereas the ν_e signal shows small invariant mass. Those events with large invariant mass are rejected.

Table 2 3) lists the number of events after this e/π^0 separation. An order of magnitude extra rejection (247.1/23) in the ν_μ neutral current background is achieved with 152.2/203.7=75% in signal acceptance.

5.2.2 Oscillation sensitivity

Figure 13 (left) shows the reconstructed neutrino energy distributions for 5 years exposure of JHF OA2°. The oscillation parameters of $\Delta m^2 = 3 \times 10^{-3}$ eV^2 and sin$^2\,2\theta_{\mu e} = 0.05$ are assumed. A clear appearance peak is seen at the oscillation maximum of E_ν ~0.75 GeV. By integrating the number of events in the energy range between 0.4 and 1.2 GeV, 90% and 3σ limits are derived as a function of the exposure time (the right plot of Figure 13). The reach of the first phase is as good as sin$^2\,2\theta_{\mu e} = 0.003$ at 90% confidence level. The systematic uncertainty in background subtraction is chosen to be 2%, 5% and 10%. Though the systematic uncertainty is not important in the first phase, it becomes significant in the second phase.

Figure 14 shows 90%C.L. contours for 5 year exposure of each beam configuration assuming 10% systematic uncertainty in background subtraction.

The best sensitivity at around $\Delta m^2 = 3 \times 10^{-3}$ eV^2 is given by OA2° and the sensitivity is sin$^2\,2\theta_{\mu e} = 0.003$ at 90%C.L. If the Δm^2 is significantly larger or smaller than $3 \times$

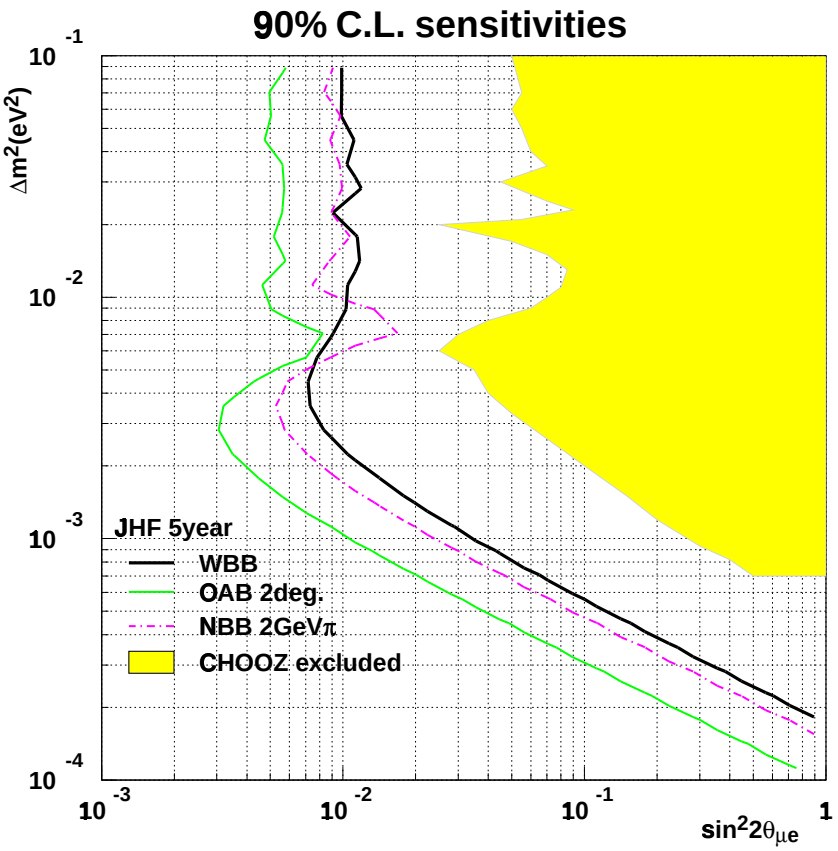

Figure 14: The 90% C.L. sensitivity contours for 5 years exposure of WBB, OA2°, and LE2π configurations. The 90% C.L. excluded region of CHOOZ is plotted as a comparison. For CHOOZ contour, maximum mixing of $\sin^2\theta_{23} = 0.5$ is assumed to convert from $\sin^2 2\theta_{13}$ to $\sin^2 2\theta_{\mu e}$.

10^{-3} eV^2, the sensitivity can be optimized by adjusting the neutrino energy as described in section 3. In the predicted range of 1.6×10^{-3} eV^2 $< \Delta m^2 < 4 \times 10^{-3}$ eV^2 by the Super-Kamiokande, the sensitivity is better than $\sin^2 2\theta_{\mu e} = 0.005$ or $\sin^2 2\theta_{13} = 0.01$ at 90% confidence level.

5.3 Confirmation of $\nu_\mu \to \nu_\tau$ in atmospheric neutrino observation

Neutral current (NC) interaction detects the sum of $\nu_\mu \to \nu_e, \nu_\mu$, and ν_τ oscillations[2]. Therefore, NC measurement combined with $\nu_\mu \to \nu_e$ and $\nu_\mu \to \nu_\mu$ measurements provide indirect measurement of the $\nu_\mu \to \nu_\tau$ oscillation. The NC measurement also provides a constraint on the existence of a sterile neutrino, ν_s, since the $\nu_\mu \to \nu_s$ oscillation results in reduction of NC interactions.

In the JHF neutrino beam energy of $\sim$1 GeV, the dominant ν_μ NC interactions are single π productions. Among those, single π^0 production process has a unique signature that only electromagnetic showers made by decay photons are observed without any other activities. Therefore, we focus on the single π^0 production mode.

[2]According to the LEP result, there are only 3 light active neutrinos.

Table 3: Summary of the event rate of the NC candidates. $f(X)$ is the fraction of the events from X interaction.

Beam	#NC Events	Beam exposure	$f(\nu_\mu\text{NC})$	$f(\nu_\mu\text{CC})$	$(\nu_e\text{CC})$
WBB	315	1 years	0.88	0.09	0.03
LE2π	250	5 years	0.80	0.13	0.07
OA2°	700	5 years	0.84	0.09	0.07

A background from charged current (CC) interactions with a π^0 are separated by identifying at least one muon in the final state. Muons are identified by detecting an extra Čerenkov ring or the Cherenkov photons, or by detecting the decay electrons. In the Super-Kamiokande analysis, the efficiency of detecting the decay electrons is better than 80%. Another background is from NC interactions by high energy neutrinos which are out of the oscillation maximum. Though we cannot reconstruct the initial neutrino energy for the NC interaction, the total energy deposit in the detector, called "visible energy", is used to reject high energy events. When the high energy neutrino produces multiple pions, which is the dominant process at high energy, they are further suppressed by vetoing on the extra pion rings as well as decay electrons from the $\pi^+ \to \mu^+\nu_\mu, \mu^+ \to e^+\bar{\nu_\mu}\nu_e$ decay chain.

Thus, the selection criteria are defined as follows: 1) the event must be fully contained, 2) visible energy (electron equivalent energy) must be greater than 100 MeV and less than 1500 MeV, 3) the number of rings in an event must be less than three, 4) all the rings must be electron-like and 5) no decay electron is identified.

After applying these selection criteria, about 315 events are expected to be observed in one year without neutrino oscillation for WBB. Out of 315 events, 88% are from NC interactions, 9% are from ν_μ CC interactions, and 3% are from ν_e CC interaction intrinsically in the beam. The remaining 9% events from ν_μ CC interactions is hard to be eliminated because the muon is captured by oxygen and does not decay. The results are summarized in Table 3 together with the other beam configurations.

The expected numbers of events as a function of Δm^2 are shown in Figure 15. In the figures, maximal oscillations, $\sin^2 2\theta_{23}$=1.0, is assumed. Although full mixing is assumed, expected number of events does not become 0 even at the deepest dip point. This is due to the NC interactions of high energy neutrinos. The dotted lines in each figure correspond to the 90% C.L. limit for $\nu_\mu \to \nu_\tau$ oscillations assuming a systematic uncertainty of 5%. The expected numbers of events for $\nu_\mu \to \nu_\tau$ and for $\nu_\mu \to \nu_s$ are clearly separated if the Δm^2 is larger than 2×10^{-3} for WBB, 1.5×10^{-3} for LE2π and 1×10^{-3} for OA2°.

6 Physics in the future extension with Hyper-Kamiokande

In the 2nd phase of the JHF-Kamioka neutrino experiment, the proton intensity is planned to go up to 4 MW [9]. The pion (or neutrino) production target will also be

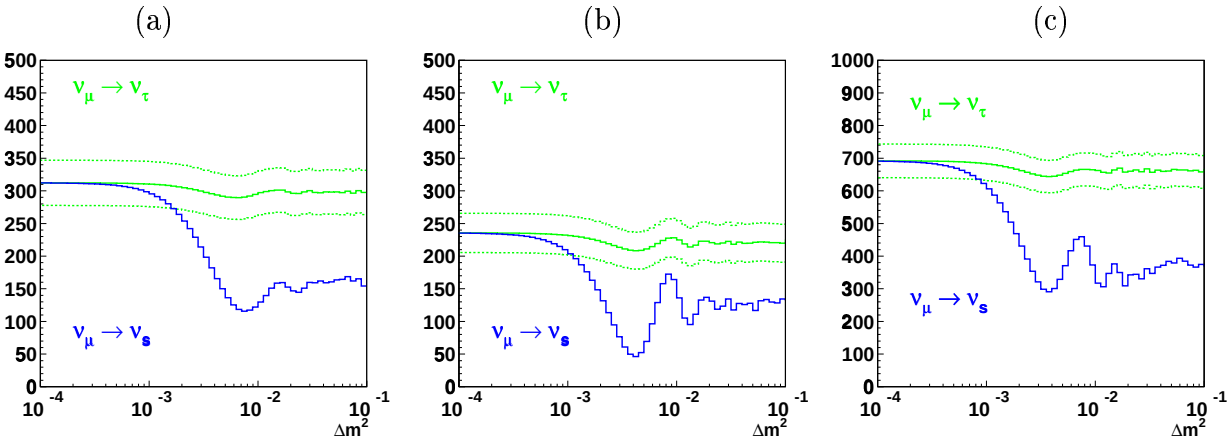

Figure 15: Expected number of events with various Δm^2 for (a) 1 year of WBB, (b) 5 years of LE2π and (c) 5 years of OA2°. The solid lines show the expected numbers of events assuming $\nu_\mu \to \nu_\tau$ or $\nu_\mu \to \nu_s$. The dotted lines show the 90% C.L. regions of $\nu_\mu \to \nu_\tau$ oscillation.

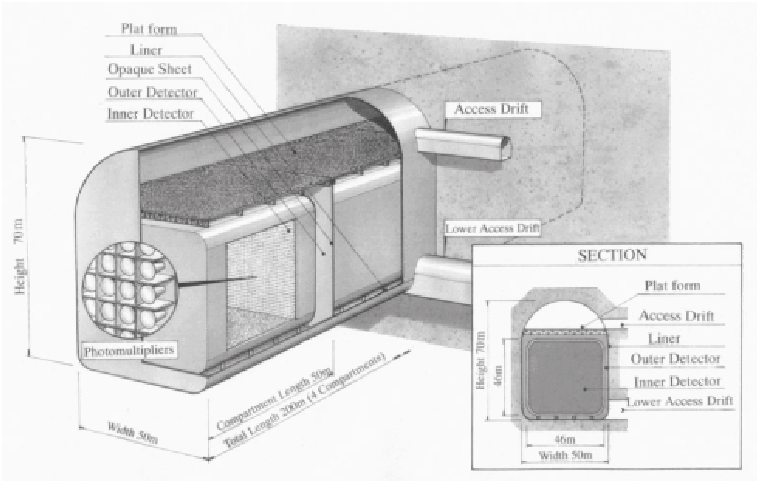

Figure 16: Schematic view of the Hyper-Kamiokande detector.

upgraded to a liquid metal target to accept the 4 MW beam. The shielding of the decay pipe will be designed to accomodate such a beam.

As for the far detector, Hyper-Kamiokande detector is proposed as a next generation large water Čerenkov detector [18] at Mozumi zinc mine in Kamioka, where the Super-Kamiokande detector is located. Schematic view of one candidate detector design is shown in Figure 16. A large water tank is made from several 50 m × 50 m × 50 m sub-detectors. The tank will be filled with pure water and photomultiplier tubes (PMTs) are instrumented on all surfaces of sub-detectors. The fiducial volume of each sub-detector is about 70 kt and 1 Mt volume is achieved by 14 sub-detectors. The 2.0 m thick outer detectors completely surround the inner sub-detectors and the outer region is also instrumented with PMTs. The primary function of the outer detectors is to veto cosmic ray muons and to help identify contained events. The Kamioka site satisfies the conditions required for constructing large water Čerenkov detectors: easy access to underground, clean water, hard and uniform rock, and infrastructure/technology for excavation. The overburden of the Hyper-Kamiokande is expected to be somewhere between 1900 and

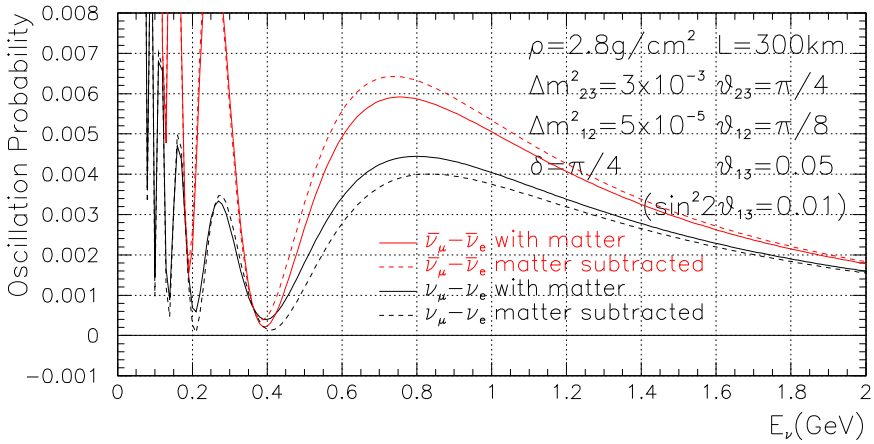

Figure 17: Oscillation probabilities for $\nu_\mu \to \nu_e$(black) and $\bar{\nu}_\mu \to \bar{\nu}_e$(red). The solid curves includes asymmetry due to matter effect. For the dashed curves, the matter effect is subtracted and the difference between $\nu_\mu \to \nu_e$(black) and $\bar{\nu}_\mu \to \bar{\nu}_e$(red) are all due to CP effect.

2700 meter-water-equivalent, depending on the actual location of the detector.

With these upgrades in both accelerator (×5) and detector (×40), the statistics is expected to increase by a factor of 200. The goal of the second phase is

- $\sin^2 2\theta_{13}$ sensitivity below 10^{-3}
- CP phase δ measurement down to 10-20 degrees
- Test of the unitarity triangle in the lepton sector
- Search for Proton decay: $p \to K^+\bar{\nu}, e^+\pi^0$

6.1 Discovery potential of CP violation in the lepton sector

If $\nu_\mu \to \nu_e$ is not observed in the first phase, another order of magnitude improvement in $\sin^2 2\theta_{\mu e}$ sensitivity to better than 10^{-3} will be performed in the second phase (Fig 13). Systematic uncertainty in background subtraction becomes important in the 2nd phase. Enhancement of the signal at the oscillation maximum and capability of measuring the background by the side-band of the oscillation pattern in the reconstructed neutrino energy distribution provide an excellent handle in controlling the systematic uncertainty.

If the large mixing angle solution of the solar neutrino deficit, which is the current favored solution, and if $\nu_\mu \to \nu_e$ is observed in the first phase, there is a good chance of observing CP violation in the 2nd phase. The CP asymmetry is calculated as

$$A_{CP} = \frac{P(\nu_\mu \to \nu_e) - P(\bar{\nu}_\mu \to \bar{\nu}_e)}{P(\nu_\mu \to \nu_e) + P(\bar{\nu}_\mu \to \bar{\nu}_e)} = \frac{\Delta m^2_{12} L}{4E_\nu} \cdot \frac{\sin 2\theta_{12}}{\sin \theta_{13}} \cdot \sin \delta$$

By choosing low energy neutrino beam at the oscillation maximum (E∼0.75 GeV and L∼295 km for JHF) the CP asymmetry is enhanced as 1/E. Taking the central value of LMA, namely $\theta_{12} = \pi/8$ and $\Delta m^2_{12} = 5 \times 10^{-5}$, and $\sin^2 2\theta_{13} = 0.01$ (1/10 of CHOOZ limit) and $\delta = \pi/4$ (half of the maximum CP effect), A_{CP} becomes as large as 25%. Matter effect, which creates fake CP asymmetry, increases linearly with the neutrino energy. Because of the use of low energy neutrinos, the fake asymmetry due to matter

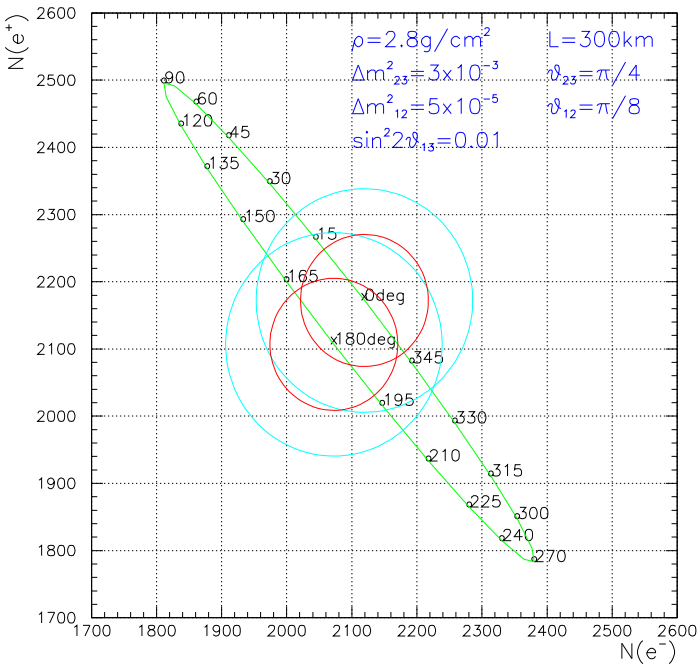

Figure 18: Numbers of ν_e and $\bar{\nu}_e$ appearance events including those from backgrounds. Two circles indicate 3σ contour (blue) and 90% confidence level (red) contours.

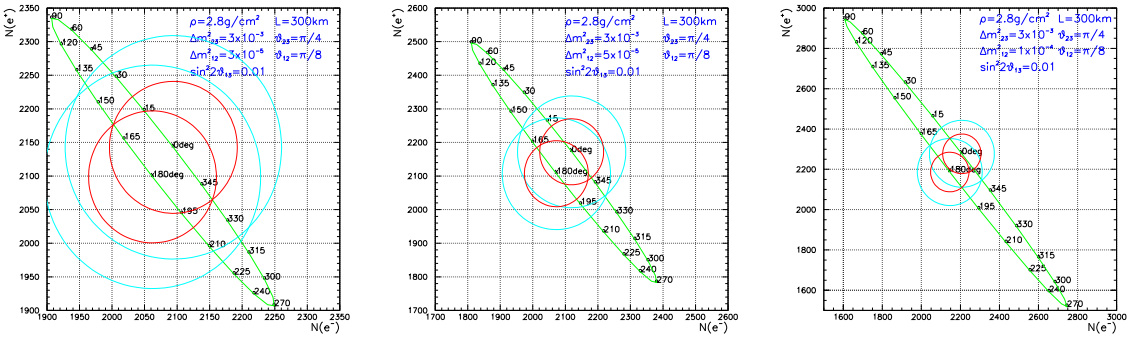

Figure 19: CP sensitivity for $\Delta m^2_{12} = 3 \times 10^{-5}$, 5×10^{-5} and 10×10^{-5}.

effect is small for the JHF-Kamioka experiment. Figure 17 shows oscillation probabilities for $\nu_\mu \to \nu_e$(black) and $\bar{\nu}_\mu \to \bar{\nu}_e$(red) for the central LMA parameters as discussed above. The solid curves includes asymmetry due to matter effect. For the dashed curves, the matter effect is subtracted and the difference between $\nu_\mu \to \nu_e$(black) and $\bar{\nu}_\mu \to \bar{\nu}_e$(red) are all due to CP effect. The CP asymmetry is as large as 25% and the fake asymmetry due to matter effect is only 5-10% as discussed above.

6.1.1 Sensitivity to CP violation and the unitarity triangle

Figure 18 shows the numbers of ν_e and $\bar{\nu}_e$ appearance events including those from backgrounds after 6 years of $\bar{\nu}_\mu$ and 2 years of ν_μ running in the 2nd phase of the JHF-Kamioka neutrino experiment. Numbers on the plots indicates CP phase δ in degrees.

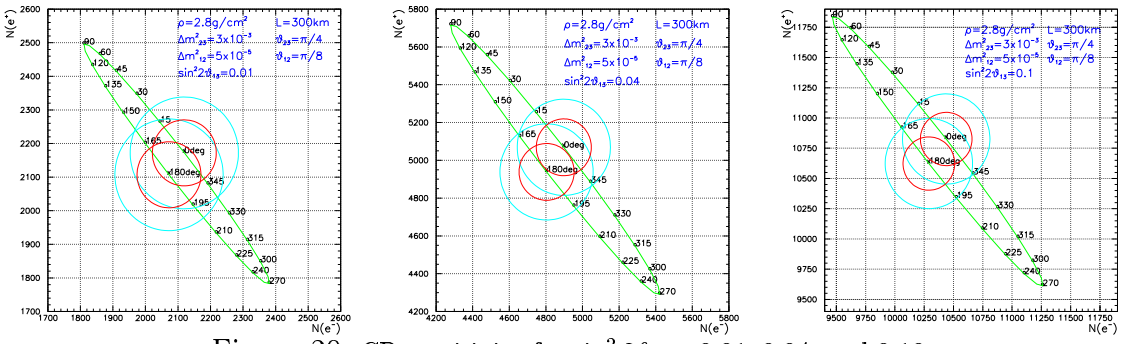

Figure 20: CP sensitivity for $\sin^2 2\theta_{13}$ =0.01, 0.04, and 0.10.

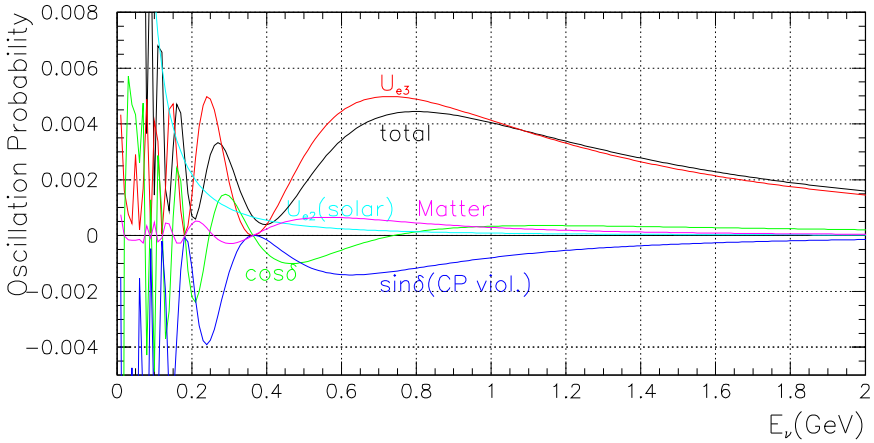

Figure 21: Contribution of different component to $\nu_\mu \to \nu_e$ appearance.

CP phase at 0 degrees and 180 degrees correspond to no CP violation. 3 sigma discovery is possible for $|\delta| > 20°$.

Figure 19 shows the CP sensitivity for $\Delta m^2_{12} = 3 \times 10^{-5}$, 5×10^{-5} and 10×10^{-5}. Because CP asymmetry (A_{CP}) increases linearly with Δm^2_{12}, CP sensitivity goes up linearly with Δm^2_{12}. For small θ_{13}, CP asymmetry increases as $1/\sin\theta_{13}$, but the statistics are down as $\sin^2\theta_{13}$. As a result, CP sensitivity does not depend much on the value of θ_{13} (for $\sin^2 2\theta_{13} > 0.01$) as shown in Figure 20. Figure 21 shows the contributions of each of the terms in $\nu_\mu \to \nu_e$ appearance for the typical LMA number discussed before. Because contribution of these terms are all significant, each of the components in Eq (11) can be determined by measuring the oscillation pattern of the $\nu_\mu \to \nu_e$ and $\bar{\nu}_\mu \to \bar{\nu}_e$ appearances. This oscillation pattern provides 4 independent measurements of the MNS matrix elements and can overconstrain the unitary triangle: $U^*_{e1}U_{\mu 1} + U^*_{e2}U_{\mu 2} + U^*_{e3}U_{\mu 3} = 0$ [19].

6.2 Sensitivity of proton decay

The existence of the neutrino oscillation indicates the extremely small neutriino masses, which is 12-13 orders of magnitude smaller than the top quark mass. A natural way to explain this hierarchy is Grand Unified theories (with see-saw mechanism), which is also indicated by the running gauge coupling constants. The only known way to directly observe the grand unification phenomenon is a nucleon decay measurement. The main

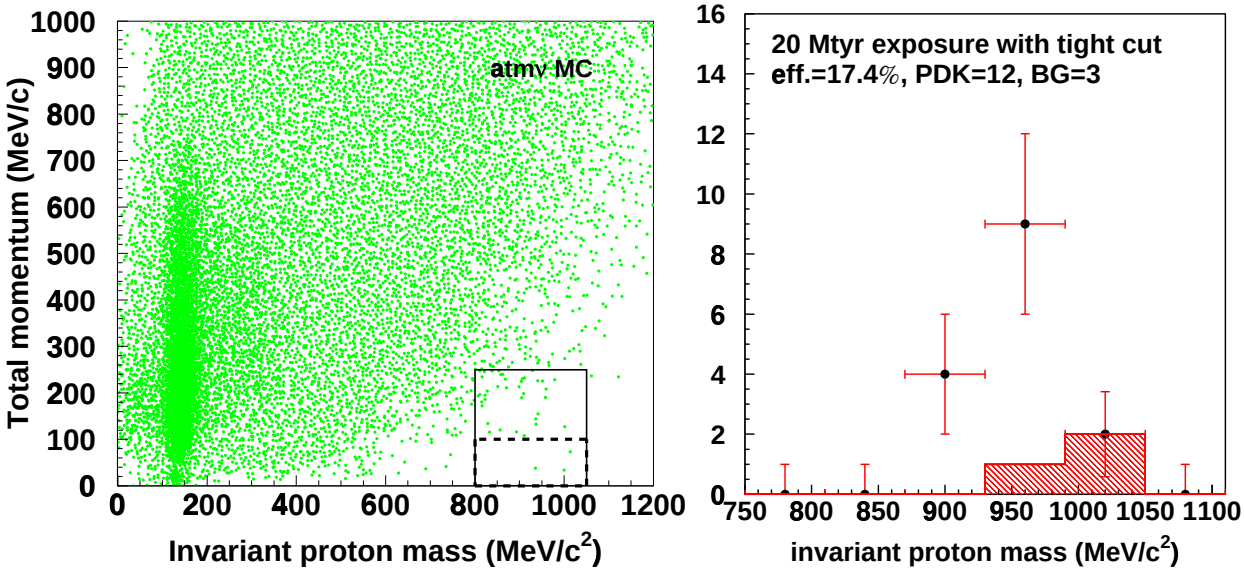

Figure 22: Left: Observed invariant proton mass and total momentum distributions for simulated atmospheric neutrino backgrounds of 20 Mt·year exposure. Solid box shows traditional selection criterion used in Super-Kamiokande [23]. Dashed box shows new tighter cut for reducing background. Right: Observed invariant proton mass distributions for 20 Mt·year exposure. Partial proton lifetime for $p \to e^+\pi^0$ is assumed to be 1×10^{35} years.

gauge-boson-mediated decay is $p \to e^+\pi^0$ and the predicted lifetime could be as short as $\sim 10^{35}$ years [20]. For supersymmetric grand unified theories, $p \to \bar{\nu}K^+$ decay tends to be the main decay mode and its predicted life time is somewhere between $10^{32} - 10^{35}$ years, although this decay mode is highly model dependent. For both of these modes, it is highly desirable to reach the sensitivity of $\sim 10^{35}$ years and beyond. Current lower limits on partial lifetimes of these two modes from 79 kton-year of Super-Kamiokande data [21] are

$$\tau_p/B_{p\to e^+\pi^0} > 5.0 \times 10^{33} \text{ years (90\% confidence level)}$$

$$\tau_p/B_{p\to \bar{\nu}K^+} > 1.6 \times 10^{33} \text{ years (90\% confidence level)}$$

where τ_p is the proton lifetime and B is the branching ratio of the decay mode.

In the following sensitivity study [22], the neutrino interaction simulation and detector simulation used in Super-Kamiokande are used. Figure 22 shows simulated atmospheric neutrino backgrounds for 20 Mt·year exposure. The solid box shows the signal region used in Super-Kamiokande [23]. An estimated number of background events is 45 for 20 Mt·year and it appears that background limits the statistics in the future $p \to e^+\pi^0$ search and a tighter cut is desired.

In the water molecule, 2 out of 10 protons are free protons. These free protons have no Fermi motion and thus give sharp proton mass peak in $e^+\pi^0$ invariant mass distribution (x-axis) and nearly perfect momentum balance (y-axis). The detection efficiency is also higher because of no pion interaction loss in the Oxygen nucleus. The dashed box in the figure represents a tighter selection criterion in momentum balance to select only the free proton decay. The background level is reduced by a factor of 15, or 3 background events/20 Mt·year), whereas the 39% of the signal detection efficiency is maintained.

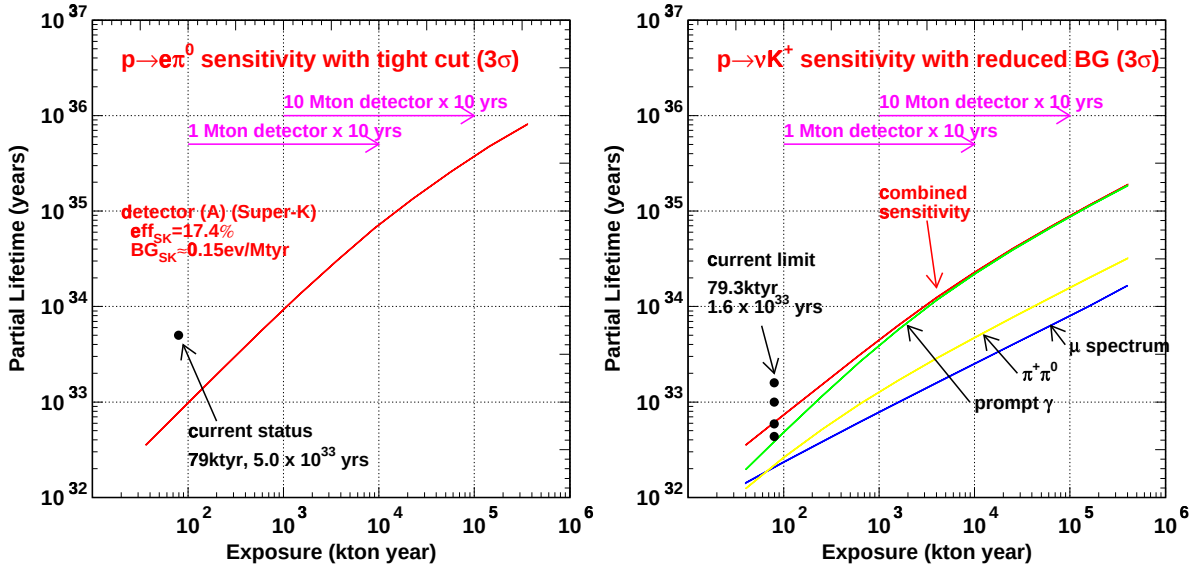

Figure 23: Expected sensitivity for the partial lifetime of protons as a function of detector exposure. In the left figure, the sensitivity for $p \to e^+\pi^0$ is calculated at 99.73%(3σ) confidence level. The tight momentum cut (see text) is used in the calculation. The right figure shows the expected sensitivity for $p \to \bar{\nu}K^+$ mode. Background is assumed to be reduced for muon and prompt gamma tagging method (see text). The upper line shows the combined sensitivity for this decay mode.

The overall signal detection efficiency is 17.4%. Figure 22(right) shows the expected invariant mass distribution for 20 Mt·year exposure data, assuming a partial lifetime for the proton of 1×10^{35} years and the tight cut described above. A sharp peak at the proton mass is seen, which would provide a redundant positive evidence of proton decay. Figure 23(left) shows 99.73%(3σ) discovery sensitivity. With 20 Mt·year exposure, we will reach a sensitivity beyond 10^{35}years.

For the $p \to \bar{\nu}K^+$ search, Super-Kamiokande developed a nearly background free method of detecting μ^+ from a $K \to \mu\nu$ decay accompanied by a prompt γ from the residual oxygen nucleus [24]. The backgrounds for this prompt γ tagging is assumed to come from kaon production by atmospheric neutrinos. Figure 23(right) shows 99.73%(3σ) discovery sensitivity for the $p \to \bar{\nu}K^+$ search. With 20 Mt·year exposure, we will reach a sensitivity of 3×10^{34}years, closing (or opening?) the windows for many of the supersymmetric grand unified theories.

7 Summary

The next generation long baseline neutrino experiment from JHF to Super Kamiokande with a baseline length of 295 km is proposed to explore the physics beyond the Standard Model. The JHF PS is designed to be capable of delivering 3.3×10^{14} protons every 3.42 seconds (0.77 MW), which is upgradeable to more than five times greater intensity (4 MW) later. The high intensity neutrino beam is produced with a conventional method. Low energy narrow band beam whose peak energy is tuned to the oscillation maximum of ∼0.8 GeV is used to maximize the sensitivity on the neutrino oscillation. Super-Kamiokande has very a good energy resolution and excellent particle identification

at this low energy. The neutrino energy is reconstructed through quasi-elastic interaction, which is a dominant process for the neutrino energy of below 1 GeV. The experiment will be divided into two phases. The goals for the first phase are precision measurements of oscillation parameters in ν_μ disappearance, search for ν_e appearance, a confirmation of $\nu_\mu \to \nu_\tau$ oscillation by detecting neutral current events, and search for sterile neutrinos. The expected precision and reach are estimated by using 1) the neutrino flux and spectrum obtained by the simulation code of neutrino beam production used by the K2K experiment, 2) Super-Kamiokande's full detector simulator which has been tested in detail over the last &5 years for the atmospheric neutrino observation. The expected precision is $\delta(\sin^2 2\theta_{23}) \sim 0.01$, $\delta(\Delta m^2_{23})$. 1×10^{-4} eV^2 in ν_μ disappearance and ν_e appearance can be explored down to $\sin^2 2\theta_{\mu e} \sim 3 \times 10^{-3}$. In the second phase of the experiment with an upgraded 4 MW PS and 1 Mt Hyper-Kamiokande, ν_e appearance can be searched for in the region $\sin^2 2\theta_{13} < 5 \times 10^{-4}$ and CP violation can be observed if $|\delta|$ & $10 - 20^\circ$ in the case of large mixing angle solution of the solar neutrinos. Sensitivity in the proton decay search is significantly improved upto 10^{35} (3×10^{34}) years in life time for the $p \to e^+\pi^0$ ($p \to \bar{\nu}K^+$) mode. The first phase experiment is planned to start in 2007.

References

[1] Super-Kamiokande collaboration, Phys.Rev.Lett. 81,1562 (1998)

[2] K2K collaboration, hep-ex/0103001, accepted for publication in Phys. Lett. **B**.

[3] Z. Maki, M. Nakagawa, S.Sakata, Prog. Theor. Phys. 28,870 (1962)

[4] M.Kobayashi, T. Maskawa, Prog. Theor. Phys. 49,652 (1973)

[5] Y. Fukuda et al., Phys. Rev. Lett. **81**, 1562 (1998); K. Kaneyuki, talk presented at 2001 Aspen winter conference on particle physics *"PARTICLE PHYSICS AT THE MILLENNIUM"*, Jan. 2001.

[6] The Super-Kamiokande collaboration, hep-ex/0103032, hep-ex/0103033, to appear in Phys. Rev. Lett.

[7] CHOOZ: Apollonio M. et al., Phys. Lett. **B**466 (B1999) 415. Palo Verde:F. Boehm *et al.*, Nucl.Phys.Proc.Suppl.91:91-98,2001

[8] B. Richter, SLAC-PUB-8587 (hep-ph/0008222), 2000 and references there in.

[9] M. Furusaka, R. Hino, Y. Ikeda *et al.*, *"The Joint Project for High-Intensity Proton Accelerators"*, KEK Report 99-4; JAERI-Tech 99-056; JHF-99-3 (1999).

[10] For example, R. Barbieri, P. Creminelli, A. Strumia, Nucl. Phys. **B585**, 28 (2000).

[11] L. Hall, H. Murayama, N. Weiner, Phys. Rev. Lett. **84**, 2572 (2000)

[12] S. Geer, Phys. Rev. **D57**, 6989 (1998)

[13] For example, Yamanoi Y. et al., KEK Preprint 97-225, November 1997.

[14] D. Beavis, A. Carroll, I. Chiang, *et al.*, Proposal of BNL AGS E-889 (1995).

[15] R. Brun et al., CERN DD/EE/84-1 (1987).

[16] T.A.Gabriel et al., ORNL/TM-11185; C.Zeitnitz and T.A.Gabriel, Nucl. Instr. and Meth. **A349**, 106 (1994).

[17] K. Nishikawa, talk presented at KEK-PS review, Dec., 2000; T. Nakaya, talk presented at 2001 Lake Louise Winter Institute, Feb., 2001.

[18] M. Koshiba, *Phys. Rep.* **220**, 229 (1992); K. Nakamura, talk presented at Int. Workshop on Next Generation Nucleon Decay and Neutrino Detector, 1999, SUNY at Stony Brook; K. Nakamura, *Neutrino Oscillations and Their Origin*, (Universal Academy Press, Tokyo, 2000), p. 359.

[19] J. Sato, hep-ph/0008056 (2000).

[20] W. Marciano, talk presented at UNO proto-collaboration meeting, 2000, Carlsbad, USA.

[21] M. Shiozawa, talk presented at the 30th Int. Conf. on High Energy Physics (ICHEP2000), 2000, Osaka, Japan.

[22] M. Shiozawa, *Next Generation Nucleon Decay and Neutrino Detector(NNN99)* (AIP Conference Proceedings 533, AIP, New York, 2000) p.21; M. Shiozawa, talk presented at Int. Workshop on Next Generation Nucleon Decay and Neutrino Detector, 2000, Fermi National Laboratory, USA.

[23] M. Shiozawa *et al.*, *Phys. Rev. Lett.* **81**, 3319 (1998).

[24] Y. Totsuka, *7th Workshop on Grand Unification, ICOBAN '86*, (World Scientific, 1986), p. 118; Y. Hayato *et al.*, *Phys. Rev. Lett.* **83**, 1529 (1999).